Genetic architectures of floral pigment and patterning in hybrid monkeyflowers

Arielle M. Cooley[1,*], Caroline Schlutius[2], Melia Matthews[1,8], Xingyu Zheng[2,3], Daniel Thomas[1], Patrick P. Edger[4], Adrian E. Platts[4], Amy LaFountain[5], Logan George[2], Aaron Williams[1], Douglas Hundley[6], Yao-Wu Yuan[5], Alex Twyford[7] and Joshua R. Puzey[2]

[1]Biology Dept, Whitman College, Walla Walla WA, USA, [2]Biology Dept, College of William & Mary, Williamsburg VA, USA, [3]School of Biological Sciences, Cold Spring Harbor Laboratory, Cold Spring Harbor, NY 11724, USA, [4]Department of Horticulture, Michigan State University, East Lansing, MI, USA, [5]Dept of Ecology & Evolutionary Biology, University of Connecticut, Storrs CT, USA, [6]Math Dept, Whitman College, Walla Walla WA, USA, [7]School of Biological Sciences, University of Edinburgh, Edinburgh, Scotland, UK, [8]Biomedical and Biological Science Dept., Cornell University, Ithaca, NY, *Corresponding author: cooleya@whitman.edu, 345 Boyer Ave., Walla Walla WA 99362 U.S.A.

ABSTRACT

Hybridization generates inter-genomic interactions, which may result in unique traits not seen in either parent species. Here we explore the genetic basis of both carotenoid and anthocyanin floral pigmentation in hybrids between monkeyflower species *Mimulus cupreus* and *M. luteus* var. *variegatus*. *Mimulus cupreus* has abundant yellow carotenoid pigmentation in its petal lobes, while *M. l. variegatus* has a derived reduction in carotenoid intensity. Thus, as expected, carotenoid intensity segregates in an F2 hybrid population. More surprisingly, both species appear to have petal lobes solidly and identically covered in magenta anthocyanin pigment (which, when overlaid on the bright yellow carotenoid background, leads to an orange color in *M. cupreus*), yet F1 and F2 hybrids exhibit novel and complex spatial patterns of anthocyanin spotting. A rare yellow morph of *M. cupreus*, which lacks petal anthocyanins, also generates spatially patterned offspring when hybridized with *M. l. variegatus*. We use this cross, together with newly developed high-quality genome assembly of *M. l. luteus* and image analysis tools, to investigate the genetic architecture of color and pattern variation in an F2 hybrid population. We report a single QTL, containing the *Beta-carotene hydroxylase* (*BCH*) gene, associated with the non-patterned carotenoid reduction in *M. l. variegatus*. HPLC shows that relative beta-carotene abundance differs between dark yellow and light yellow petals, supporting a causal role for *BCH*. The presence versus absence of petal lobe anthocyanin segregates in a 3:1 ratio, and we report (as expected) an associated QTL encompassing the anthocyanin activator *MYB5a/NEGAN* which has previously been shown to be both necessary and sufficient to activate petal lobe anthocyanins in *M. l. variegatus*. Anthocyanin patterning was more complex, with seven QTLs associated with five quantitative patterning traits on the upper petals; 11 on the lower petals; and three qualitative whole-flower patterning traits. Although power was too limited to effectively test for epistatic interactions in this cross, the QTLs provide candidate genomic regions for further investigating the molecular mechanisms of spatially complex floral color patterning, and multiple candidate genes are identified including anthocyanin activators and an anthocyanin repressor.

KEYWORDS Anthocyanins; Carotenoid intensity; Color patterning; Digital image analysis; *Erythranthey*; Floral pigmentation; Genetic architecture; Hybrid novelty; Hybridization; *Mimulus*; monkeyflower; spatial patterning

Introduction

Hybridization between species forces two divergent genomes to co-exist within the same organism. These genomic interactions can yield surprising results at both molecular and phenotypic levels, with evolutionary consequences ranging from species

Manuscript compiled: Sunday 20th August, 2023
[2]Corresponding author: Whitman College Biology Dept., 345 Boyer Ave, Walla Walla WA, USA, cooleya@whitman.edu.

extinction (Levin *et al.* 1996; Epifanio and Philipp 2000) to adaptation (Anderson and Stebbins Jr 1954; Rieseberg *et al.* 2003; Suarez-Gonzalez *et al.* 2018), adaptive radiation (Seehausen 2004; Marques *et al.* 2019; Grant and Grant 2019), and hybrid speciation (Grant 1971; Rieseberg 1997; Mallet 2007). Finding the genetic architecture of hybrid-specific phenotypes is an important step towards understanding their origins and predicting their evolutionary trajectories.

Plant pigmentation has long served as a vehicle for investigating genomic, developmental, and evolutionary mechanisms (McClintock 1950; Davies *et al.* 2012; Sobel and Streisfeld 2013). A change in plant pigmentation can have profound ecological and evolutionary consequences, due to the diverse roles of pigment including pollinator attraction, herbivore deterrence, and protection against abiotic stressors such as light and extreme temperatures (Chalker-Scott 1999; Gould 2004; Demmig-Adams *et al.* 1996). These factors have the potential to impose selection ranging from positive to purifying (Smith *et al.* 2013; Zhao *et al.* 2014; Ho and Smith 2016), and to promote the maintenance of phenotypic variation within species (Takahashi *et al.* 2015; Sapir *et al.* 2021; Kellenberger *et al.* 2019) as well as divergence between species (Schemske and Bradshaw 1999). Overall, plant pigmentation has evolved frequently and has generated spectacular amounts of phenotypic diversity, particularly in the petals of flowering plants.

In flowers, the two major classes of pigments are the yellow-to-orange carotenoids and the red-to-purple anthocyanins (Grotewold 2006). Of these two, the anthocyanin biosynthetic pathway, and its regulation by R2R3 MYB, bHLH, and WDR transcription factors, has been more intensively characterized (Holton and Cornish 1995; Davies *et al.* 2012; Xu *et al.* 2015; Chen *et al.* 2019). However, one major aspect of anthocyanin pigmentation remains poorly understood: unlike carotenoid pigmentation, which tends to vary only in intensity or hue, anthocyanin pigmentation frequently exhibits intricate and difficult-to-quantify spatial patterns.

Patterning traits such as speckling and spotting offer an opportunity to explore fundamental principles of evolution and development, as has been done with eyespot formation in butterflies (Beldade and Brakefield (2002)), yet such traits in plants are only beginning to be addressed (Martins *et al.* (2013, 2017); Neher and Hallatschek (2013); Yamagishi *et al.* (2014); Ding *et al.* (2020)). Genetic mapping is an important tool for investigating the mechanisms by which spatial complexity evolves and develops; however, a necessary prerequisite to genetic mapping is a quantifiable phenotype. The difficulty of scoring and analyzing spatially complex variation has been a barrier to genetic and developmental analyses of many evolutionarily fascinating traits (Houle *et al.* (2010); Minervini *et al.* (2015); Gehan and Kellogg (2017)), and a variety of algorithms are now being developed to help lessen this barrier. These include machine-learning approaches as in Boogaard *et al.* (2020) and computer vision based techniques as in Galkovskyi *et al.* (2012). In plants, phenotypic image analysis has been developed for traits including color intensity (De Keyser *et al.* 2013; Trivellini *et al.* 2014; Li *et al.* 2020), leaf shape (de Souza *et al.* 2016; Weight *et al.* 2008), root characteristics (Kimura *et al.* 1999; Nakano *et al.* 2012), and overall plant architecture (Knecht *et al.* 2016). Quantitative analysis of petal patterns is still relatively uncommon, perhaps because of the sheer abundance of flower color traits that are readily categorized using "by-eye" methods. As interest in quantitative pattern variation increases, the development of new tools will be essential, because techniques developed for other types of biological traits are not easily adapted to capturing variation across a heterogeneously pigmented petal surface. Examples of digital image processes developed specifically for color patterning in plants are limited, but include Yoshioka *et al.* (2004) and Li *et al.* (2022).

An attractive biological system for studying the evolution of plant pigmentation and color patterning is the monkeyflower genus *Mimulus* (synonym *Erythranthe* (Barker *et al.* 2012; Lowry *et al.* 2019)). The genus features an abundance of floral diversity and an array of ecological, molecular, and genomic resources (Wu *et al.* 2008; Sobel and Streisfeld 2013; Yuan 2019). Anthocyanin and carotenoid pigmentation vary across *Mimulus*. Unfortunately, most of the complex color patterns are found in species that are rare, unstudied, or both. One exception is the *luteus* species group from Chile (Grant 1924; Watson and Von Bohlen 2000; Cooley *et al.* 2008), which combines ease of growth in the greenhouse, a solid foundation of prior ecological and pigmentation research (Esterio *et al.* 2013; Medel *et al.* 2007; Cooley *et al.* 2011; Zheng *et al.* 2021), ease of hybridization (Stanton *et al.* 2016), and an intriguing hybrid-specific petal pattern phenotype. The *luteus* group consists of the broadly distributed *M. luteus* var. *luteus*, as well as *M. l. variegatus*, *M. naiandinus*, *M. cupreus*, and *M. depressus*, all of which have more limited distributions in mid- to high-elevation regions of the Andes mountains (Von Bohlen 1995).

The *luteus* group has long been thought to have polyploid origins. The species in the group have approximately doubled chromosome counts relative to the diploid *Mimulus guttatus*, with n = 30, 31, or 32, compared to n = 14 or 15 for *M. guttatus* (Mukherjee and Vickery 1962; Vickery *et al.* 1968; Vickery 1995). Chromosome pairing in F1 hybrids between *M. luteus* var. *luteus* and *M. guttatus* points to allo- rather than autopolyploidy: one half of the *M. l. luteus* chromosomes pair with *M. guttatus* chromosomes, in the F1, while the other half of the *M. l. luteus* chromosomes remain unpaired. This lack of pairing between the two subgenomes of *M. l. luteus*, also observed in chromosome squashes of pure *M. l. luteus* (Mukherjee and Vickery 1960), is consistent with observations that traits and markers segregate in a simple diploid fashion in this and other members of the *luteus* group (Cooley and Willis 2009; Cooley *et al.* 2011).

More recently, genomic analyses have corroborated the allopolyploidy hypothesis. The 640-680 Mb *M. l. luteus* genome contains 46,855 identified protein-coding genes (Edger *et al.* 2017), approximately twice the 26,718 protein-coding genes found in the 430 Mb *M. guttatus* genome (Hellsten *et al.* 2013). Most *M. guttatus* genes have two identifiable homeologs in *M. l. luteus*. Two subgenomes, "A" and "B", were identified within *M. l. luteus*, and in 1853 of 2200 gene trees (84.2%), subgenome A was more closely related to *M. guttatus* than it was to subgenome B (Edger *et al.* 2017). As with the chromosome-pairing evidence, this last observation indicates that the whole-genome duplication shared by members of the *luteus* group most likely arose from a hybridization event between a *M. guttatus*-like ancestor and an unidentified, non-*guttatus*-like ancestor.

The *luteus* group is nested within the *Simiolus* section of *Mimulus*, which is characterized almost uniformly by yellow-flowered plants displaying red dots of anthocyanin pigment in the nectar guide region of the flower (Grant 1924). In the *luteus* group, in contrast, flower color has evolved dramatically (Fig. 1A). The overall color visible to the human eye can be yellow, orange, red, or pink, depending on the abundance of the yellow carotenoid

pigments versus the magenta anthocyanin (specifically, cyanidin) pigment (Cooley *et al.* 2008).

Petal carotenoids have been lost or greatly downregulated in petals of the white-and-pink flowered *M. naiandinus* and the magenta-flowered *M. l. variegatus* (Cooley and Willis 2009). The two carotenoid reductions are genetically distinct: recessive in *M. naiandinus* versus semi-dominant in *M. l. variegatus* compared to *M. l. luteus* (Fig. 1D: compare yellow intensity of *naiandinus* x *luteus* F1s to *variegatus* x *luteus* F1s).

Petal lobe anthocyanin (PLA) pigmentation, meanwhile, has been gained in *M. naiandinus*, *M. l. variegatus*, and *M. cupreus* (Cooley and Willis 2009). In each case, the presence of PLA is dominant to its absence (determined by crosses to both *M. l. luteus* and the yellow morph of *M. cupreus*), and segregates in a 3:1 ratio in an F2 hybrid population. PLA has been gained at least twice independently, evidenced by its mapping to two different genomic regions - *pla1* for *M. naiandinus* and the common orange morph of *M. cupreus*, and *pla2* for *M. l. variegatus* (Cooley and Willis 2009; Cooley *et al.* 2011). A rare yellow morph of *M. cupreus*, found at only a single locality, likely represents a secondary loss of petal lobe anthocyanins, and a complementation test indicates that the causal locus is in the *pla1* region (Cooley and Willis 2009).

Hybridization reveals an unexpected property of the anthocyanin pigmentation in *M. l. variegatus* versus *M. cupreus*: hybrids are characterized by a spatially complex distribution of petal anthocyanin pigmentation not seen in either parent (Fig. 1B-D). This patchy color patterning is seen regardless of whether the cross involves the common orange morph of *M. cupreus* (high carotenoids and high anthocyanins), or the rare yellow morph (high carotenoids but no petal lobe anthocyanins) (Fig. 1B-D).

Genetic mapping (Cooley *et al.* 2011) and functional genetic experiments (Zheng *et al.* 2021) indicate that the R2R3 MYB transcription factor gene *MYB5a/NEGAN* at genomic region *pla2* is responsible for the gain of petal anthocyanin in *M. l. variegatus*, while *pla1* - which contains a series of seven tandemly arrayed MYB genes - is responsible for the gain of petal anthocyanin in the orange-flowered morph of *M. cupreus* and its subsequent loss in the yellow morph. Interestingly, crosses to a third taxon (*M. l. luteus*) that lacks petal anthocyanins reveal underlying pattern differences between *M. l. variegatus* and *M. cupreus*. Using *M. l. variegatus* as the anthocyanin donor yields F1 hybrids with a "globular" phenotype of large patches of petal anthocyanin. In contrast, using the orange morph of *M. cupreus* as the anthocyanin donor yields F1 hybrids with a faint anthocyanin layer referred to here as the "blush" phenotype (Fig. 1D). Such observations suggest cryptic divergence in patterning between these two apparently solid colored species.

To help investigate the intricate patterns seen in the hybrids, we developed digital tools for quantifying color patterning on a petal surface, along with a new and highly improved *M. l. luteus* reference genome. Using these resources, we were able to identify seven QTLs associated with 19 patterning traits. As expected, the presence versus absence of anthocyanin pigment, which segregates in a simple 3:1 ratio in this and other crosses (Cooley and Willis 2009; Cooley *et al.* 2011), maps to a QTL at *pla2*, containing the anthocyanin-activator gene *MYB5a*. We also identify one QTL contributing to the unpatterned variation in yellow carotenoid intensity. This QTL encompasses a beta-carotene processing candidate gene and covaries with petal beta-carotene concentration relative to the abundance of other carotenoid pigments. Collectively, our results provide a first step towards understanding the multifaceted genetic basis of coloration in *Mimulus* hybrids.

Materials and Methods

Plant materials and growth conditions

Two highly inbred lines, *Mimulus luteus* var. *variegatus* RC6 and *M. cupreus* LM43 (Table 1), were grown in the Whitman College greenhouse under 14-hour days with daily misting from an automatic watering system. Temperatures ranged from approximately 10-15 °C overnight and 15-30 °C during the day. Pollen from *M. cupreus* LM43 was applied to *M. l. variegatus* stigmas to generate F1 hybrid seeds. F1 plants were raised in the Whitman College greenhouse and manually self-fertilized to generate F2 hybrid seeds. The cross was performed in only one direction, because previous work indicated that cross direction does not influence color patterning traits in either an F1 or F2 hybrid population of *variegatus* x *cupreus* (Cooley and Willis 2009). F2 plants were grown in two locations: the Whitman College greenhouse, and the College of William & Mary greenhouse. At the latter location, plants were grown under 16 hour light regimen at 18-25 °C. *Mimulus l. luteus* line EY7 was grown at the College of William & Mary and was used for preparation of a reference genome.

Petal photography and qualitative trait assessment

Each *Mimulus* flower consists of five petals: two dorsal (upper), two lateral, and one ventral (lower) petal (Fig. 1). In many *Mimulus* species, including those studied here, the lower petal differs from the other four in that it has a series of anthocyanin spots leading from the petal lobe into the throat. These spots appear to act as nectar guides.

We examined both upper petals of each flower, considering them to be approximate (though mirror image) replicates of the same pattern. We also examined the lower petal, hypothesizing that the genes which pattern the nectar guide region might alter how color patterns are produced throughout this unique petal, compared to any of the other petals.

From each of 2-4 flowers per F2 plant, the two upper petals and the lower petal were cut at the base within 48 hours of flower opening. Petals were placed on a strip of white tape and photographed in a darkroom. A single 60-watt soft white (2700K) bulb was used to provide illumination. Each photo included a color standard and a ruler. Photographs were taken using an Olympus VG-120 digital camera (Whitman College), and a Nikon D3200 (William and Mary). Each photograph was cropped and rotated in Gimp v. 2.10.8 (https://www.gimp.org/) so that only the tape background and petals were visible. The resulting .jpg image was processed using the digital image analysis pipeline described below.

Using the photographs, nine traits were scored "by eye" based on visual assessment by a single individual (Table 2). For these traits, a single score was assigned to each flower rather than to each petal. To evaluate repeatability, a set of 100 images was later scored by a second individual for four representative traits. Images were scored identically for the binary traits of blush, globular spray, and fine spray in 85, 92, and 87 out of 100 images respectively. The fourth tested trait, carotenoids, had three levels and yielded identical scores in only 66 out of 100 cases, suggesting a lower degree of repeatability.

Digital image analysis pipeline

To enhance downstream analysis of flower photos, full-color photos were first transformed to a 3-color space (L*a*b* (014-4/E 2007)), using k-means clustering with 3 centroids: red for anthocyanin-pigmented petal tissue, yellow for non-anthocyanin-pigmented petal tissue, and white for the background (Fig. 2). Using a custom script in combinaton with the Matlab plotter, clustering was supervised with manual repositioning of color centroids to ensure optimum retention of detail of spot shapes. Color categorization was implemented in Matlab version 2017b (MATLAB 2017). Two traits - proportion red on the upper petals, and proportion red on the lower petal - were calculated directly in Matlab for each petal, then averaged across petals and flowers to obtain a single upper-petal value and a single lower-petal value per plant.

Further image analysis was undertaken using a custom pipeline (Fig. 2) implemented within the SciPy Ecosystem (Virtanen *et al.* 2020), with tools from the Scikit Image (Van der Walt *et al.* 2014) and Shapely (Gillies *et al.* 2007–) packages. In brief, spots and petals were vectorized to polygons from rasters using the Marching Squares (Cubes) algorithm (Lorensen and Cline 1987); holes in spots were detected with a custom algorithm; and all polygons were checked for validity and repaired if possible. Repairs to polygons were implemented by both automated methods based on Shapely validation tools, and a series of manual correction programs based on the Matplotlib pyplot framework. These manual curations also acted as a final quality control step for vector images. All petal polygons were assigned a unitless area of one, and spot sizes were scaled relative to this total area, to allow generalized comparisons among flower petals and images of different sizes. Several programs for hand-curation of spot and petal vectors were created and used to ensure final image quality.

The final set of vectors representing the petal, spots, and holes-within-spots, were saved by the pipeline as geojson files that are readable with standard GIS software. Following the conversion of photos to vectors, spots were counted and measured in relation to the size of their respective petals and their position within the petals. These measurements were then used as quantitative phenotypic traits in the QTL experiment.

Code for the python image processing package is available on github at:<github.com/danchurch/mimulusSpeckling>. It is also available at pypi.org: <pypi.org/project/makeFlowerPolygons-dcthom/> A guided tour to the use of the pipeline is available as a jupyter notebook at: <nbviewer.jupyter.org/github/danchurch/mimulusSpeckling/blob/master/make_polygons/notebooks/petals_to_polygons.ipynb>.

A total of 90 petal spot traits were computationally measured, to assess the features listed in Table 3 for both upper petals and lower petals (45 traits each) for genetic mapping. Within a plant, for a given petal type (upper petals or lower petal), each phenotype was separately averaged to give a single value per plant for the upper petals or lower petal. A total of 353 unique plants were assessed, of which 310 were ultimately used for genetic mapping.

Assembly of the M. l. luteus reference genome

To improve the assembly of the draft *M. l. luteus* genome (Edger *et al.* 2017), we generated new long-read and long-range genomic sequencing data. Using *Mimulus luteus* var. *luteus* line EY7, we first reduced levels of secondary compounds by maintaining plants in the dark for several days, then extracted high molecular weight DNA. The DNA was sequenced using the Sequel II platform, to obtain approximately 35x genome-wide PacBio HiFi coverage. A HiC library was constructed and sequenced to approximately 100x, using 150 bp short reads generated via Illumina NovaSeq, to aid in scaffolding. The primary assembly was constructed using Hifiasm (https://github.com/chhylp123/hifiasm; Cheng *et al.* (2021)) with primarily default parameters (except -D 10) to assemble PacBio highly accurate long reads (HiFi reads) into a set of contigs with a low probability of chimerism between subgenomes.

Next, HiC reads were aligned to the primary assembly with bwa (mem) and processed with SALSA 2.2 (https://github.com/marbl/SALSA) to generate a scaffolded assembly. Analysis of synteny (COGE synmap) with the diploid *M. guttatus* suggested that read alignment included some misalignments between subgenomes and this had been incorporated into the scaffolding. We therefore moved away from bwa to novoalign for HiC alignments with parameters (-r None -t 30) selected to reject any alignments with even a low chance of alignment ambiguity.

To aid in annotation, RNA was extracted from young floral and vegetative buds and sequenced using PacBio IsoSeq. The resulting assembly was annotated using two rounds of Maker with a transcriptome input generated using stringtie (https://ccb.jhu.edu/software/stringtie/) in reference guided long-read mode based on a set of *M. l. luteus* IsoSeq reads, together with the *M. guttatus* v5.0 proteome from Phytozome 12 (https://phytozome.jgi.doe.gov/pz/portal.html) and a repeat library generated on the assembly using repeatModeler (https://www.repeatmasker.org/RepeatModeler/). HMMs for Augustus (http://bioinf.uni-greifswald.de/augustus/) and SNAP (https://github.com/KorfLab/SNAP) were initially trained on *M. guttatus* gene models and then retrained on the first round *M. l. luteus* maker gene models, while geneMark used the standard eukaryotic gene models. Genome statistics were generated using the assemblathon stats (https://github.com/KorfLab/Assemblathon/) code and assembly/annotation completeness was assessed using BUSCO v4 (https://busco.ezlab.org/) with Eudicot odb10 models in genome and proteome modes respectively. Completeness assessment with the recently released BUSCO v5 code did not significantly change these results.

QTL Mapping

Fresh leaf tissue (0.09 - 0.10 g per leaf) was collected from each of 353 *M. l. variegatus* RC6 x yellow *M. cupreus* LM43 F2 plants whose petals had been photographed (see "Petal photography and pattern quantification"). Tissue was snap frozen in liquid nitrogen. DNA was extracted using a Qiagen DNeasy Plant Mini Kit (Germantown, MD, USA), double eluted in 30-35 uL of warm dH20, and checked for purity and concentration using either a Nanodrop Lite (Thermo Fisher Scientific, Waltham, MA, U.S.A.) or a Qubit 4 Fluorometer (Invitrogen, Carlsbad, CA, U.S.A.). Genotyping by Sequencing (GBS) libraries were prepared following the protocol of Elshire *et al.* (2011). In brief, 100 ng of DNA was digested with the frequent cutting enzyme ApeKI prior to the ligation of a unique forward adaptor and a standard common adaptor. Up to 95 samples and a water control were subsequently pooled prior to PCR amplification.

Three lanes of Illumina HiSeq 100 bp single-end sequencing

were performed by the Duke University Center for Genomic and Computational Biology. Sequences were demultiplexed using Stacks version 2.1 (Catchen *et al.* 2011) and aligned to the *M. l. luteus* genome using bowtie2 and SNPs were called using GATK HaplotypeCaller. The resultant VCF file was filtered to remove sites with greater than 50% missing data, converted into a HapMap using Tassel, and than processed with the Tassel 'run_pipeline.pl' to convert HapMap to csv. The 'run_pipeline.pl' script filters the SNP dataset to include locations that meet the following cutoffs: (1) the parents were genotyped and (2) the parental genotype is not heterozygous. (https://bitbucket.org/tasseladmin/tassel-5-source/wiki/UserManual/GenosToABH/GenosToABHPlugin). A total of 7767 sites survived this filtering.

The resultant CSV file was used in R/qtl to create linkage groups and conduct QTL mapping (Broman *et al.* 2003). To create linkage groups, the data was further filtered to remove individuals with more than 250 missing marker calls and remove markers with more than 100 missing individuals. Next, duplicate individuals, defined as those who shared greater than 75% identity at markers, were removed from the dataset. Finally, markers with distorted segregation patterns (as determined by cutoff of p<1e-5) were filtered. Using this filtered dataset, we estimated recombination fractions between alleles, formed linkage groups, and reordered markers using this newly formed linkage map. Markers were not forced to match the *M. l. luteus* genome but were driven by patterns of recombination.

We used R/qtl to carry out QTL mapping for the carotenoid and anthocyanin traits shown in Tables 2 and 3, as well as upper- and lower-petal proportion red. QTL were identified using the R/qtl 'scanone' function, with the 'em' method and 1000 permutations. A 'binary' model was used for the manually scored phenotypes while a 'normal' model was used for the computationally measured phenotypes. We attempted to detect epistatic interactions, however, given that only 239 of our samples possessed pigment, our power for detecting interactions was limited. For traits that were scored by-eye, all individuals that did not produce pigment were excluded from the analysis. For traits that were computationally measured, we performed two analyses – one including all individuals and a second excluding individuals that lacked pigment as determined by the by-eye analyses. Overall, the QTL analysis of computationally measured traits that excluded individuals that lacked significant pigment (as determined by-eye) had less power to detect QTLs. As a result, the QTL analysis of computationally measured traits presented here includes all individuals.

After QTL mapping, we identified all markers passing significance. For each of these markers, we broadened the identified peak to approximately 25 cM away on each side. Protein sequences corresponding to BCH (from *A. thaliana*), RTO in *Mimulus*, and previously identified Mybs related to Anthocyanin activation were BLASTed against the newly assembled *M. luteus* genome. The location of the top BLAST hits were determined with the linkage map. The each location of the gene within the linkage map was limited by marker resolution.

Carotenoid extraction and analysis

Carotenoids were extracted from ventral petals of yellow-flowered *M. cupreus* and *M. cupreus* x *M. l. variegatus* F1 hybrids, as well as from a series of four F2 hybrids that display pigmentation ranging from pale to dark yellow (Fig. 5). The petal area used for each extraction was standardized by closing a 1.5 mL Eppendorf tube over the petals to create a "punch". Two punches per flower were placed in 200 ul of methanol and ground with a nylon pestle until the tissue appeared colorless.

The ground tissue was centrifuged at 16,000 g for 1 min to pellet debris, after which the supernatant was transferred to a clean Eppendorf tube. Carotenoids and flavonoids were then partitioned by adding 150 ul of methylene chloride and 150 ul of distilled water to each tube. The carotenoid-containing layer (i.e., lower phase) of selected samples was collected and dried under a gentle stream of nitrogen gas. The dried extracts were treated with ethanolic potassium hydroxide to remove fatty acid esters according to the methods of Schiedt (1995). Saponified carotenoids were dried under nitrogen gas, redissolved in 9:1 (v/v) hexanes/acetone and chromatographed according to the method outlined in LaFountain *et al.* (2015).

Carotenoids were identified based on their absorption spectra and relative order of elution as compared to a previously published analysis (LaFountain *et al.* 2015). The relative percentages of each carotenoid per sample were determined by integrating the area under each carotenoid peak (Waters Empower 2.0 Software), manually correcting for differences in their extinction coefficients (Britton 1995) and comparing each value to the total carotenoid content.

Data availability

File S1 contains trait data obtained from digital image analysis. File S2 contains the phenotypes measured by eye. File S3 contains the genotypes used in QTL mapping. File S4 contains QTLs identified and Percent Variation Explained (PVE) associated with each QTL. Sequence data will become available on GenBank upon publication. The Python image processing package is available on github at <github.com/danchurch/mimulusSpeckling>. Raw sequencing data (fastq files) used in QTL mapping will be available in SRA upon publication. Seeds of inbred lines are available upon request.

Results

Chromosome-level assembly of the M. l. luteus reference genome

The newly assembled *Mimulus luteus* genome size of 599 Mb, with a scaffold L50 of 32 and N50 of 6.4 Mb, compares favorably with estimates for the genome size of 640-680 Mb made by flow cytometry and a previous assembly of 410 Mb that had a scaffold N50 of 0.28 Mb (Edger *et al.* 2017). Notably, this revised assembly appears to incorporate both more duplicated polyploid gene space and pericentromeric sequence space missing from the previous *luteus* assembly and the assembly of the diploid relative *M. guttatus* (JGI version 5.0, Phytozome-13: MguttatusTOL551v5.0) respectively (Fig. 3). The distribution of Ks scores from a self-self synmap alignment validates the rich history of genome duplications previously described in *M. l. luteus* (Vickery 1995).

Consistent with a more complete polyploid gene space, the maker annotation gene count increased to 53,411 genes from 46,855 in the previous assembly and approaches twice the *M. guttatus* diploid protein-coding gene count (2x26,718(guttatus): 53,436). The similarity of these two values may be somewhat coincidental since the short read *M. guttatus* assembly was likely depleted in gene space relative to the long-read *M. luteus* assembly, whilst diploidization will have begun to reduce the gene count in *M. luteus*, bringing these two values together. Missing BUSCO genes remained around 2.5%, similar to the level in the previous assembly (2.6%).The *luteus* assembly contains

significant blocks of sequence without evident CDS homology in the assembled *M. guttatus* genome (Fig. 3), although similar sequence can be found in unassembled *M. guttatus* BAC and clone sequence available in genbank. The size of these gene-poor blocks missing from the *M. guttatus* assembly ranges up to c. 10 Mb, and is consistent with the incorporation of more complete centromeric and pericentromeric sequence in the long-read *M. luteus* assembly. However, tandem duplicate arrays make scaffolding of these regions with HiC reads more prone to error than HiC scaffolding of chromosome arm regions.

Carotenoid intensity maps to a QTL containing candidate gene Beta-carotene hydroxylase

Carotenoid levels in the petal lobes were visually assessed as low, medium, or high levels of yellow pigment (Fig. 2), with *M. l. variegatus* displaying the derived trait of carotenoid reduction. Color variation was less pronounced in the nectar guide region, where light-flowered F2s still retained visible amounts of carotenoid pigmentation.

Petal lobe carotenoids mapped to a QTL on linkage group 4 (Fig. 4), which contains one known carotenoid-related gene: the biosynthetic enzyme gene *Beta-carotene hydroxylase* (*BCH*). Mean trait values were consistent with an additive genetic mechanism. Plants with a heterozygous genotype for a marker at the center of QTL-4 were significantly lighter than plants with a homozygous *cupreus* genotype, and significantly darker than plants with a homozygous *variegatus* genotype (Fig. 5).

Carotenoid composition changes with pigment intensity

Liquid-liquid phase partitioning of flavonoids and carotenoids, depicted in Fig. 7, reveals that the yellow pigmentation of these flowers is due to carotenoids. Flavonoid-based pigments (e.g., anthocyanins or chalcones) would be expected to migrate to the aqueous (upper) layer but were not observed in these samples. Carotenoids are expected to migrate to the methylene chloride (lower) layer. The range of yellow pigmentation observed in the lower layer of these samples corresponds to their respective floral colors, providing strong support that this pigmentation is carotenoid-based.

To further interrogate the identity of these pigments, the extracts from the *M. cupreus*, *M. cupreus* x *M. l. variegatus* F1 hybrids, and darkest and lightest F2 hybrids, were separated by high-performance liquid chromatography (HPLC). These data reveal that all flowers sampled can synthesize the xanthophylls produced by the late carotenoid biosynthetic pathway enzymes (e.g., neoxanthin, deepoxyneoxanthin, and mimulaxanthin; Fig. 7). However, the F1 and light F2 individual show an increased relative concentration of beta-carotene, as would be expected if an early carotenoid biosynthesis pathway structure gene such as *BCH* were disrupted.

Genetic mapping recovers the pla2 anthocyanin presence/absence locus

Consistent with Cooley and Willis (2009), we observed a 3:1 ratio of petal lobe anthocyanin (PLA) presence versus absence in our mapping population, with 228 out of 310 (73.5%) of the F2 plants showing the dominant *variegatus* phenotype of anthocyanin production in the petal lobes. Transcriptional activator *MYB5a/NEGAN* has previously been shown to be both necessary and sufficient for PLA (Zheng *et al.* 2021), and is located at the center of QTL-3a, in the region marked *pla2* (Fig. 4).

Along with this "by-eye" trait of PLA presence versus absence, a total of 20 patterning traits mapped to QTL-3a. The association of so many patterning traits with QTL-3a is presumably due to the substantial differences in the traits' values between plants with versus without PLA pigmentation.

Three markers unlinked to QTL-3a (at QTL-5b and QTL-16) appeared to be marginally associated with the presence versus absence of PLA. This finding, together with the central marker at QTL-3a explaining only 19% of variation in PLA (File S4), is unexpected for a trait that segregates in a perfect single-locus Mendelian fashion, as PLA does in this cross. Possible explanations include false positives, marker-trait recombination, and/or misplaced markers in the linkage map.

Anthocyanin pigment, when present, is patterned by at least seven genes

In addition to the *MYB5a/NEGAN*-containing QTL-3a, seven other anthocyanin-related QTLs were discovered (Fig. 4). Peaks on linkage groups 1, 3, 5, 6, and 11 were each associated with 1-3 patterning traits (Fig. 5). The QTL on linkage group 17 (QTL-17) was associated with nine total traits: the "by-eye" trait of tip spot presence vs. absence; one upper-petal trait; and seven lower-petal traits (Fig. 6).

Significant overdominance, in which the trait value of the heterozygote exceeds that of either parental genotype, was detected for QTL-1 (Fig. 5). Plants heterozygous for a marker near the center of QTL-1 had a significantly higher proportion of lower-petal spots in Quadrant 3, which is in the distal portion of the petal, compared to plants homozygous for either allele. QTL-5a showed a similar trend towards overdominance, for the proportion of lower-petal spots in Quadrant 2 (on the proximal half of the petal). The *cupreus* allele was dominant to the *variegatus* allele for the QTL-3b (proportion of upper-petal spots on Quadrant 4), but was recessive for all of the other mapped anthocyanin traits.

One trait, "fine spray," was only detected when the dataset was filtered to remove the 25% of plants that lack Petal Lobe Anthocyanin (PLA) pigmentation, and even then was at the border of statistical significance (File S4). For all other traits, we found that the power to detect QTLs was higher when the PLA-lacking plants were not filtered out.

The *pla1* genomic region is responsible for activating anthocyanin pigmentation in the orange-flowered morph of *M. cupreus*, but not in the yellow-flowered morph used in this cross. Nonetheless, *pla1* was contained within one of our mapped QTLs: QTL-17, which is the locus (after QTL-3a) that associates with the largest number of traits. The *pla1* region contains seven tandemly-arrayed MYB genes, all of which belong to the anthocyanin-activating "subgroup 6" of the MYB gene family (Stracke *et al.* 2001; Cooley *et al.* 2011), and all of which may be candidate genes for anthocyanin-related variation.

One other potential anthocyanin candidate gene was discovered: a homolog of *RED TONGUE* (*RTO*) at QTL-11, which is predictive of the number of spots at the base of both upper and lower petals. In other *Mimulus* species, *RTO* has been shown to be a repressor of *MYB5a/NEGAN*, contributing to anthocyanin spotting as part of a Turing-type reaction-diffusion system in which *MYB5a/NEGAN* initiates spot formation and *RTo* limits spot size by inhibiting *MYB5a/NEGAN* (Ding *et al.* 2020).

Discussion

Interspecies hybrids expand the range of phenotypic variation seen in nature, presenting opportunities to investigate traits that are not typically found in existing species. Here we investigate

the genetic architecture of a classic, spatially simple interspecies difference in yellow carotenoid pigmentation as well as that of a spatially complex anthocyanin pigmentation phenotype that emerges only in interspecies hybrids.

A single QTL was found in association with the evolutionarily recent carotenoid reduction in *M. l. variegatus*. The QTL encompasses the carotenoid biosynthetic gene *Beta-carotene hydroxylase-1* and covaries with the petal concentration of beta-carotene relative to other carotenoid pigments. The paler yellow yellow pigmentation of *M. l. variegatus* appears to be caused at least in part by a shift towards a higher relative abundance of beta-carotene compared to other types of carotenoid pigments.

The gain of petal lobe anthocyanin (PLA) pigmentation in *M. l. variegatus* was, as expected, associated with a QTL encompassing the previously-identified causal gene *MYB5a* (Zheng *et al.* 2021). The *MYB5a* gene appears to be responsible for activating anthocyanin in the nectar guide regions of many *Mimulus* species (Ding *et al.* 2020). In *M. l. variegatus*, it has expanded its expression into the petal lobe regions, where it switches on continuous anthocyanin pigmentation (Zheng *et al.* 2021).

When this dominant *variegatus* allele of *MYB5a* activates PLA in hybrids, in contrast, it generates spatially complex patterns. Amongst the 3/4 of F2 plants exhibiting PLA, we were able to identify seven QTLs, collectively associated with 19 patterning traits.

In the course of investigating the genetic basis of color patterning, new resources were developed for the plant research community. The substantially improved, high-quality *M. l. luteus* genome will contribute to genetic research within the *luteus* group as well as to comparative studies across *Mimulus*. This will open up new opportunities to investigate questions around the repeated evolutionary outcomes of shifts in flower color and pigmentation patterns, as well as polyploid history and the retention and expression of duplicated gene copies. The digital image analysis pipeline adds to the repertoire of tools available for studying complex spatial patterns in plants, an area that has been less accessible to geneticists compared to more qualitative traits.

BCH is a strong candidate for the evolution of reduced carotenoid pigmentation in M. l. variegatus

The carotenoid-based variation in yellow intensity in the petal lobes was mapped to a QTL that contains the *Beta-Carotene Hydroxylase* gene (*BCH*). *BCH* is a particularly promising candidate gene for two reasons. (i) The dark yellow genotypes, including the *M. cupreus* parent and dark yellow F2s, accumulate no beta-carotene but a mixture of xanthophylls that are downstream of beta-carotene in the flower petals, whereas the light yellow genotypes, including the *M. cupreus* x *M. l. variegatus* F1 hybrid and pale yellow F2 individuals, accumulate beta-carotene as a major carotenoid component (Fig. 7). This is consistent with a low level of *BCH* activity in the light yellow genotypes, as *BCH* is the enzyme converting beta-carotene to downstream xanthophylls. (ii) *BCH* is not only a key enzyme determining the relative composition between beta-carotene and downstream xanthophylls, but also underlies major QTLs explaining total carotenoid content variation in other plant systems. For example, *BCH* was implicated as the causal gene underlying the Y-locus determining potato tuber flesh color (yellow vs. white); elevated expression level of *BCH* is tightly associated with yellow flesh color (Kloosterman *et al.* 2010). Similarly, *BCH* expression level was found to be a major determinant of petal carotenoid content variation among *Ipomoea* species (Yamamizo *et al.* 2010).

How *BCH* activity affects total carotenoid accumulation is unknown. One possibility is that higher activity increases metabolic flux into the carotenoid biosynthesis pathway, and hence leads to higher carotenoid production (Zhou *et al.* 2011). Another possibility is that chromoplasts in some plants have better storage capacity for esterified carotenoids than beta-carotene (Ariizumi *et al.* 2014). Since *BCH* catalyzes the addition of hydroxyl residues to beta-carotene and these hydroxyl groups are required for carotenoid esterification, *BCH* activity could affect total carotenoid accumulation by enhancing carotenoid storage in chromoplasts. Carotenoid intensity is likely not a single-locus trait, and additional QTLs could potentially be discovered by both increasing the size of the genetic mapping population and utilizing a quantitative phenotyping tool such as digital image analysis.

Transcriptional activator MYB5a/NEGAN underlies the anthocyanin presence/absence QTL

In flowering plants, the anthocyanin biosynthetic pathway that produces red to purple pigments is regulated by an "MBW" complex consisting of a subgroup-6 R2R3 MYB transcriptional activator and bHLH and WDR cofactors (Petroni and Tonelli 2011). Color patterning changes have frequently been tracked to the anthocyanin-activating subgroup 6 R2R3 MYB genes (Yuan *et al.* 2014; Streisfeld *et al.* 2013; Lowry *et al.* 2012; Yamagishi 2013; Schwinn *et al.* 2006; Twyford *et al.* 2018). The evolutionarily recent and genetically dominant gains of petal lobe anthocyanin pigmentation, in both the the common orange morph of *M. cupreus* and the magenta-flowered *M. l. variegatus*, follow this pattern. Pigment gain has been mapped in each case to a single genomic region (*pla1* and *pla2* respectively). Each genomic region spans a tandem array of subgroup 6 R2R3 MYB genes, and the "activating" allele at each region is associated with higher expression of the late biosynthetic genes that are the targets of the MBW complex (Cooley *et al.* 2011).

The *pla1* genomic region is responsible for petal lobe anthocyanin (PLA) in the orange morph of *M. cupreus*. In the present study, we used a rare yellow-flowered morph of *M. cupreus* that lacks the anthocyanin-activating allele at *pla1* (Cooley *et al.* 2011), likely due to a large deletion in candidate gene *MYB2* (Orr et al. unpublished manuscript: https://www.biorxiv.org/content/10.1101/2022.12.11.519905v4). Thus, all anthocyanin activation in our genetic mapping population is expected to be caused by the dominant *M. l. variegatus* allele of the *pla2* genomic region. Consistent with this expectation of single-gene control, approximately a quarter of all F2 plants (82/310) lacked petal lobe anthocyanin, having presumably inherited two copies of the recessive *M. cupreus pla2* allele.

Within *pla2*, a combination of transgenic overexpression, RNAi, and transcriptomics has identified *MYB5a* as the causal gene for petal lobe anthocyanin activation in *M. l. variegatus* (Zheng *et al.* 2021). As expected, this gene lies directly underneath QTL-3a, which associates with anthocyanin presence versus absence. More surprisingly, a small peak on linkage group 5 and a single marker on linkage group 16 show linkage to PLA. Given the robustly single-locus segregation of anthocyanin presence versus absence in this and previous crosses, we suspect that the QTL-5b and QTL-16 might represent either false positives or misplaced markers.

Seven QTLs contribute to pattern variation

QTL-3a appears to act as a single-locus "switch" controlling petal lobe anthocyanin presence versus absence. It is also associated with 20 other traits. However, this association is likely an artefect: variation in these traits is expected to be dominated by the complete lack of petal lobe anthocyanin pigment in one quarter of our F2 plants. In future work, focusing research effort on plants with the dominant anthocyanin-present phenotype will maximize statistical power to detect QTLs that contribute to quantitative pattern variation.

In addition to QTL-3a, we identified seven anthocyanin patterning QTLs. Three predicted variation in by-eye traits: the presence versus absence of blush (QTL-5b), fine spray (QTL-6), and tip spots (QTL-17). All seven QTLs, meanwhile, were associated with more subtle shifts in pigment distribution captured by our image analysis pipeline, highlighting the utility of quantitative approaches to capture variation that may be missed by categorical methods.

Several of the patterning QTLs were barely above the significance threshold, and thus might not be repeatably captured without very large sample sizes. Some of these might be false positives. An alternative (and, in our opinion, likely) explanation is that much of the pattern variation identified here is underlain by many small-effect loci.

In several cases - QTL-5a, QTL-6, and QTL-11 - the upper petal and lower petal versions of a trait both mapped to the same QTL. This result increases our confidence in QTLs 5a, 6, and 11. It also indicates a partly shared genetic program for patterning, between the upper and lower petals. Other QTLs, however, appeared to be unique to the upper petals only (QTL-3b) or to the lower petals only (QTL-1 and most of the QTL-17 traits).

Because patterning is found in hybrids but not in either parent, it must be caused by interactions between the *M. l. variegatus* and *M. cupreus* genomes. These interactions could be between alleles of a single gene, or between *variegatus* and *cupreus* alleles at two or more loci. With our modest sample size of only 228 anthocyanin-pigmented F2s, a scan for epistasis did not reveal any notable patterns, possibly due to the low statistical power. However, we did detect statistically significant single-locus intergenomic interactions for QTL-1, as well as a near-significant trend for one of the two traits mapping to QTL-5a (Fig. 5). In each case, the heterozygous genotype has a higher trait value than either parental genotype, while the two parental genotypes are statistically equivalent. Both QTLs are associated with the spatial distribution of spots, although in opposite directions. At QTL-1, the heterozygous genotype shows a high proportion of spots in Quadrant 3, which is in the distal half of the petal, while the heterozygous genotype at QTL-5a correlates with a high proportion of spots in Quadrant 2, which is in the proximal half.

Many of the QTLs appear to be capturing a shift in the overall spatial distribution of spots - from petal center to edge, or proximal to distal, or relative to a single quadrant of the petal. This suggests that the definition of distinct zones within the petal may be a key developmental aspect of spot formation. Indeed, spatial gradients of signaling molecules have long been thought to dictate the localization of developmental features (Crick 1970). In animal bone development, for example, this is achieved via spatial gradients of diffusible morphogens such as BMPs (Bier and De Robertis 2015). Graded distributions are also key to plant development, particularly involving the plant hormone auxin (Tanaka *et al.* 2006), but spatial gradients of transcription factors are also well documented (Mähönen *et al.* 2014). We speculate that some of the QTLs associated with regional anthocyanin spot formation may ultimately be traced, not to a member of the anthocyanin-producing gene network, but to a gene that encodes a diffusible protein expressed early in petal development, or to a gene involved in regulating diffusible signaling molecules such as auxin. Intriguingly, however, our results do also leave open the possibility of the involvement multiple paralogous MYB transcription factors - not just in the activation of petal lobe anthocyanins by *MYB5a*, but in patterning that pigment when present. The seven *MYB* genes located at *pla1*, in QTL-17, are all excellent candidates for influencing pattern formation, possibly by interacting with *MYB5a* (QTL-3a) and/or *RTO* (QTL-11) as part of a Turing-type reaction-diffusion system.

The variation in all of the patterning traits that we mapped was quite subtle - virtually unobservable by eye, and with relatively slight differences in mean trait values across QTL genotypes. This was true even for the binary and simple-to-score trait of "tip spots," which were clearly either present or absent in each F2 plant. Tip spots mapped to linkage group 17, but that QTL was not the sole determinant of the trait: the likelihood of a plant having tip spots increased from 8.2% in a *v/v* homozygote to only 26.3% in the recessive *c/c* homozygote. This recessive *cupreus* allele had similarly modest effects on the other eight traits mapping to QTL-17, slightly though significantly increasing the proportions of spots located at petal edges and tips (Fig. 6). This may speak to a probabilistic underlying mechanism rather than a highly deterministic one, or to a complex genetic basis of which QTL-17 is but one component.

It is notable that we did not identify any QTLs relating to total spot number or size. Although F2 plants clearly differed strikingly in these two traits (Fig. 1C), the genetic component of variation may be small and/or highly multi-locus, rendering them difficult to map. Larger sample sizes, or alternative approaches such as bulk segregant analysis (Li and Xu 2022), might be useful in discovering the genetic bases of these major yet elusive components of pattern variation. Alternatively, the phenotypes themselves may be less reliably estimated by our image analysis pipeline than the other traits that we measured. In plants with large total amounts of pigmentation, in particular, substantial spot overlap complicates the detection of individual spots. Recombinant Inbred Lines (RILs) are currently in development, and will enable crosses between phenotypes that differ in spot number and size, yet have little enough total anthocyanin pigmentation that spot overlap is minimized.

Conclusions

Hybrids can be intermediate in phenotype to their two parents; similar to only one parent; or, in some cases, entirely different from what would be predicted based on the parents' appearance. Here we present an intriguing example of the latter case, in the monkeyflower genus *Mimulus*. We show that the genetic architecture of a hybrid-specific anthocyanin color patterning trait is complex, with at least seven QTLs contributing to pattern variation. The fact that patterned petal anthocyanin pigmentation is seen only in hybrids indicates an important role for inter-genomic interactions, and indeed we identified one case of significant overdominance, at QTL-1. Additional interactions may be multi-locus, and thus detectable only with the large sample sizes required for epistasis scans of complex traits. Most of the anthocyanin QTLs reported here are associated with regional variation in spot formation across the petal surface, pointing towards zone formation in early-developing petals as a potentially

important determinant of hybrid color patterning.

Acknowledgements

We thank former William & Mary undergraduate Matthias Leu and former Whitman undergraduate Taylor Wilke, for earlier work that helped pave the way for ideas explored in this paper. Funding was provided by NSF-DEB 1655311 (to AMC), NSF-DEB 1754075 (to AMC and JRP), NSF-IOS 2031272 (to AMC and JRP), Whitman College, and the College of William & Mary.

Literature Cited

014-4/E, I. S., 2007 Cie 1976 l*a*b* colour space. Joint ISO/CIE Standard: Colorimetry-Part4 .

Anderson, E. and G. L. Stebbins Jr, 1954 Hybridization as an evolutionary stimulus. Evolution **8**: 378–388.

Ariizumi, T., S. Kishimoto, R. Kakami, T. Maoka, H. Hirakawa, *et al.*, 2014 Identification of the carotenoid modifying gene pale yellow petal 1 as an essential factor in xanthophyll esterification and yellow flower pigmentation in tomato (s olanum lycopersicum). The Plant Journal **79**: 453–465.

Barker, W., G. Nesom, P. M. Beardsley, and N. S. Fraga, 2012 A taxonomic conspectus of phrymaceae: a narrowed circumscription for mimulus, new and resurrected genera, and new names and combinations. Phytoneuron **39**: 1–60.

Beldade, P. and P. M. Brakefield, 2002 The genetics and evo–devo of butterfly wing patterns. Nature Reviews Genetics **3**: 442.

Bier, E. and E. M. De Robertis, 2015 Bmp gradients: A paradigm for morphogen-mediated developmental patterning. Science **348**: aaa5838.

Boogaard, F. P., K. S. Rongen, and G. W. Kootstra, 2020 Robust node detection and tracking in fruit-vegetable crops using deep learning and multi-view imaging. Biosystems Engineering **192**: 117–132.

Britton, G., 1995 Uv/visible spectroscopy. Carotenoids Vol 1B: Spectroscopy pp. 13–62.

Broman, K. W., H. Wu, Ś. Sen, and G. A. Churchill, 2003 R/qtl: Qtl mapping in experimental crosses. Bioinformatics **19**: 889–890.

Catchen, J. M., A. Amores, P. Hohenlohe, W. Cresko, and J. H. Postlethwait, 2011 Stacks: building and genotyping loci de novo from short-read sequences. G3: Genes, genomes, genetics **1**: 171–182.

Chalker-Scott, L., 1999 Environmental significance of anthocyanins in plant stress responses. Photochemistry and photobiology **70**: 1–9.

Chen, L., B. Hu, Y. Qin, G. Hu, and J. Zhao, 2019 Advance of the negative regulation of anthocyanin biosynthesis by myb transcription factors. Plant physiology and biochemistry .

Cheng, H., G. T. Concepcion, X. Feng, H. Zhang, and H. Li, 2021 Haplotype-resolved de novo assembly using phased assembly graphs with hifiasm. Nature methods **18**: 170–175.

Cooley, A., G. Carvallo, and J. Willis, 2008 Is floral diversification associated with pollinator divergence? flower shape, flower colour and pollinator preference in chilean mimulus. Annals of Botany **101**: 641–650.

Cooley, A. M., J. L. Modliszewski, M. L. Rommel, and J. H. Willis, 2011 Gene duplication in mimulus underlies parallel floral evolution via independent trans-regulatory changes. Current Biology **21**: 700–704.

Cooley, A. M. and J. H. Willis, 2009 Genetic divergence causes parallel evolution of flower color in chilean mimulus. New Phytologist pp. 729–739.

Crick, F., 1970 Diffusion in embryogenesis. Nature **225**: 420–422.

Davies, K. M., N. W. Albert, and K. E. Schwinn, 2012 From landing lights to mimicry: the molecular regulation of flower colouration and mechanisms for pigmentation patterning. Functional Plant Biology **39**: 619–638.

De Keyser, E., P. Lootens, E. Van Bockstaele, and J. De Riek, 2013 Image analysis for qtl mapping of flower colour and leaf characteristics in pot azalea (rhododendron simsii hybrids). Euphytica **189**: 445–460.

de Souza, M. M., F. N. Medeiros, G. L. Ramalho, I. C. de Paula Jr, and I. N. Oliveira, 2016 Evolutionary optimization of a multiscale descriptor for leaf shape analysis. Expert Systems with Applications **63**: 375–385.

Demmig-Adams, B., A. M. Gilmore, and W. Adams 3rd, 1996 Carotenoids 3: in vivo function of carotenoids in higher plants. The FASEB Journal **10**: 403–412.

Ding, B., E. L. Patterson, S. V. Holalu, J. Li, G. A. Johnson, *et al.*, 2020 Two myb proteins in a self-organizing activator-inhibitor system produce spotted pigmentation patterns. Current Biology .

Edger, P. P., R. Smith, M. R. McKain, A. M. Cooley, M. Vallejo-Marin, *et al.*, 2017 Subgenome dominance in an interspecific hybrid, synthetic allopolyploid, and a 140-year-old naturally established neo-allopolyploid monkeyflower. The Plant Cell **29**: 2150–2167.

Elshire, R. J., J. C. Glaubitz, Q. Sun, J. A. Poland, K. Kawamoto, *et al.*, 2011 A robust, simple genotyping-by-sequencing (gbs) approach for high diversity species. PloS one **6**: e19379.

Epifanio, J. and D. Philipp, 2000 Simulating the extinction of parental lineages from introgressive hybridization: the effects of fitness, initial proportions of parental taxa, and mate choice. Reviews in Fish Biology and Fisheries **10**: 339–354.

Esterio, G., R. Cares-Suárez, C. González-Browne, P. Salinas, G. Carvallo, *et al.*, 2013 Assessing the impact of the invasive buff-tailed bumblebee (bombus terrestris) on the pollination of the native chilean herb mimulus luteus. Arthropod-Plant Interactions **7**: 467–474.

Galkovskyi, T., Y. Mileyko, A. Bucksch, B. Moore, O. Symonova, *et al.*, 2012 Gia roots: software for the high throughput analysis of plant root system architecture. BMC plant biology **12**: 116.

Gehan, M. A. and E. A. Kellogg, 2017 High-throughput phenotyping. American Journal of Botany **104**.

Gillies, S. *et al.*, 2007– Shapely: manipulation and analysis of geometric objects.

Gould, K. S., 2004 Nature's swiss army knife: the diverse protective roles of anthocyanins in leaves. BioMed Research International **2004**: 314–320.

Grant, A. L., 1924 A monograph of the genus mimulus. Annals of the Missouri Botanical Garden **11**: 99–388.

Grant, P. R. and B. R. Grant, 2019 Hybridization increases population variation during adaptive radiation. Proceedings of the National Academy of Sciences **116**: 23216–23224.

Grant, V., 1971 *Plant Speciation*. Columbia University Press.

Grotewold, E., 2006 The genetics and biochemistry of floral pigments. Annu. Rev. Plant Biol. **57**: 761–780.

Hellsten, U., K. M. Wright, J. Jenkins, S. Shu, Y. Yuan, *et al.*, 2013 Fine-scale variation in meiotic recombination in mimulus inferred from population shotgun sequencing. Proceedings of the National Academy of Sciences **110**: 19478–19482.

Ho, W. W. and S. D. Smith, 2016 Molecular evolution of anthocyanin pigmentation genes following losses of flower color. BMC evolutionary biology **16**: 1–10.

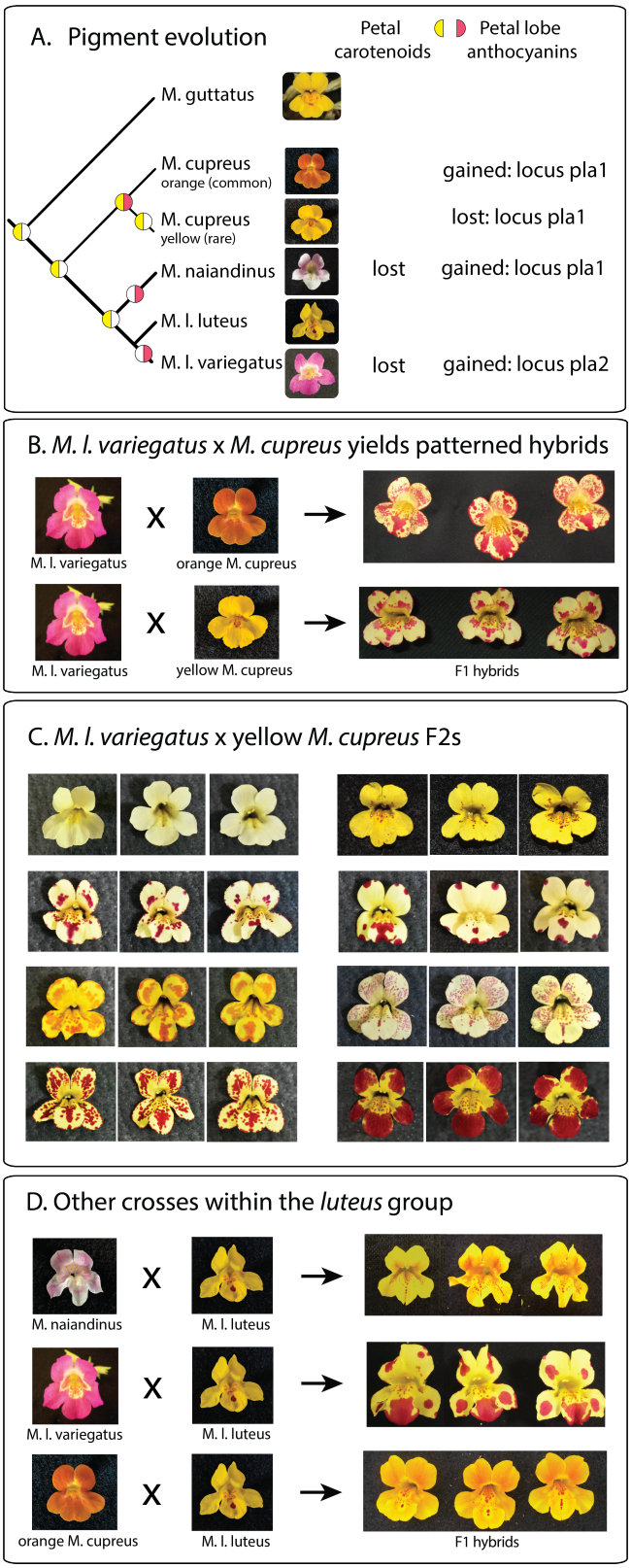

Figure 1 Flower color divergence yields complex spatial patterning in *Mimulus* hybrids. A. Because the *luteus* group is nested within a large monophyletic grouping of yellow-flowered species, the ancestral state is inferred to consist of yellow, carotenoid-pigmented petals (indicated by yellow color in the left side of the circle) with no petal lobe anthocyanins (indicated by a lack of magenta color in the right side of the circle). Carotenoids are hypothesized to have been lost twice independently, while anthocyanins are hypothesized to have been gained three times and lost once. B. Crosses are shown with maternal parent first; no differences were observed between reciprocal crosses. Three flowers per plant are shown for each F1 hybrid to illustrate the degree of consistency across flowers of the same genotype. C. Three flowers per plant are shown for each of 8 different F2 hybrids derived from the *M. l. variegatus* x yellow-flowered *M. cupreus* cross. D. Other crosses within the *luteus* group yield "blush" phenotypes or solid circles of anthocyanin pigmentation in the F1 hybrids. Photos courtesy Bella Rivera, Joshua Shin, Leah Samuels.

Table 1 Seed sources

Taxon	Line ID	Inbreeding	Population	Location[a]
M. luteus var. *luteus*	Mll-EY7	13 generations	El Yeso	33.4°S, 70.0°W (2600 m)
M. luteus var. *variegatus*	Mlv-RC6	13 generations	Río Cipreses	34.2°S, 70.3°W (1200 m)
M. cupreus yellow morph	Mcu-LM43	10 generations	Laguna del Maule	36.0°S, 70.3°W (2300 m)

[a] Locations from which seeds were collected is given as latitude, longitude (meters above sea level.

Table 2 Qualitative traits utilized in genetic mapping

Trait name	Description
Carotenoid intensity	Darkness of yellow petal pigment, scored as low, medium, or high.
Anthocyanin presence	Binary indicator of whether any anthocyanin pigment is present on the petal lobes outside of the nectar guide region.
Blush	Binary indicator of whether any of the petals had a very thin layer of diffuse anthocyanin pigment.
Tip spot	Binary indicator of whether the two upper (dorsal) petals have a single spot at the tip of the petal.
Rim spots	Amount of rim covered by spots, scored as low, medium, or high.
Huge Spot	Binary indicator of whether there is a spot that covers nearly all of the petal.
Column	Binary indicator of whether majority of the central column of the lower (ventral) petal is anthocyanin pigmented.
Fine spray	Binary indicator of whether there is a spray of small spots, coming up from the throat on the two upper (dorsal) petals.
Globular spray	Binary indicator of whether there is a spray of large spots coming up from the throat on the two upper (dorsal) petals.

Table 3 Quantitative traits utilized for genetic mapping. Each trait was measured in three petals per flower (two upper and one lower).

Trait category	Trait name	Trait description
Spot characteristics	SpotBiggest	Area of the largest detected spot
	SpotSmallest	Area of the smallest detected spot
	SpotMean	Mean area of all spots
	SpotMedian	Median area of all spots
	SpotNumber	Total number of spots on petal
Center zone	CenterNumWithin	Number of spots contained entirely in the center zone
	CenterNumTouch	Number of spots touching the center zone
	CenterNumMostly	Number of spots with a majority of their area in the center zone
	CenterNumCentroids	Number of spots whose center of mass is located in the center zone
	CenterProp1	Proportion of total spot area in center zone
	CenterProp2	Proportion of center zone covered by spots
	CenterDist1	Mean distance between spot centers of mass and the center of all spots
	CenterDist2	Mean distance between spot centers of mass and the center of only the spots that are located in the center zone
Edge zone	EdgeNumWithin	Number of spots entirely contained in edge zone
	EdgeNumTouch	Number of spots touching edge zone
	EdgeNumTouch2	Number of spots touching actual petal edge (not the edge zone)
	EdgeNumMostly	Number of spots with a majority of their area in the edge zone
	EdgeProp1	Proportion of total spot area in edge
	EdgeProp2	Proportion of edge zone covered by spots
	EdgeProp3	Proportion of length of petal edge (not edge zone) covered in spots
	EdgeDist1	Mean distance between the petal rim and the closest edge of each spot
	EdgeDist2	Mean distance between the petal rim and each spot's center of mass
Throat	ThroatNumTouch	Number of spots touching throat zone
	ThroatNumTouch2	Number of spots touching the petal base
	ThroatNumMostly	Number of spots mostly in throat zone
	ThroatProp1	Proportion of total spot area in throat
	ThroatProp2	Proportion of throat zone covered by spots
Petal regions: "X" indicates that each trait was measured for proximal and distal petal halves, and for Quadrants 1-4	X Num	Number of spots with centers of mass in Region X
	X Prop1	Proportion of total spot area in Region X
	X Prop2	Proportion of Region X covered by spots

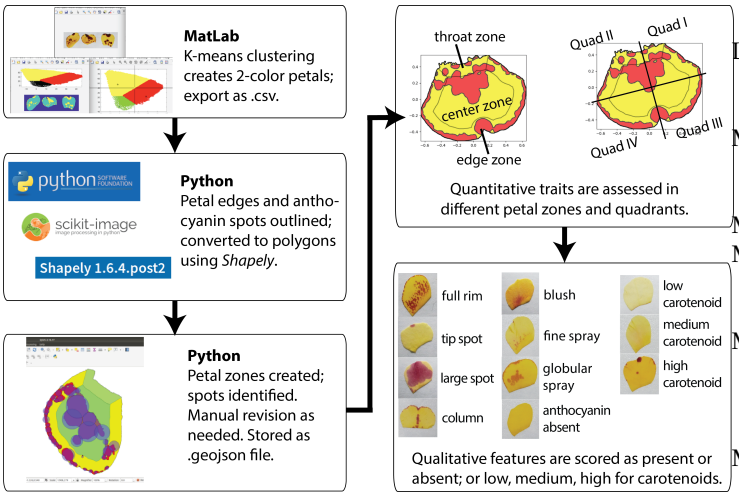

Figure 2 Digital image analysis workflow.

Holton, T. A. and E. C. Cornish, 1995 Genetics and biochemistry of anthocyanin biosynthesis. The Plant Cell **7**: 1071.

Houle, D., D. R. Govindaraju, and S. Omholt, 2010 Phenomics: the next challenge. Nature reviews genetics **11**: 855–866.

Kellenberger, R. T., K. J. Byers, R. M. D. B. Francisco, Y. M. Staedler, A. M. LaFountain, *et al.*, 2019 Emergence of a floral colour polymorphism by pollinator-mediated overdominance. Nature communications **10**: 1–11.

Kimura, K., S. Kikuchi, and S.-i. Yamasaki, 1999 Accurate root length measurement by image analysis. Plant and Soil **216**: 117–127.

Kloosterman, B., M. Oortwijn, J. Uitdewilligen, T. America, R. de Vos, *et al.*, 2010 From qtl to candidate gene: genetical genomics of simple and complex traits in potato using a pooling strategy. BMC genomics **11**: 1–16.

Knecht, A. C., M. T. Campbell, A. Caprez, D. R. Swanson, and H. Walia, 2016 Image harvest: an open-source platform for high-throughput plant image processing and analysis. Journal of experimental botany **67**: 3587–3599.

LaFountain, A. M., H. A. Frank, and Y.-W. Yuan, 2015 Carotenoid composition of the flowers of mimulus lewisii and related species: implications regarding the prevalence and origin of two unique, allenic pigments. Archives of biochemistry and biophysics **573**: 32–39.

Levin, D. A., J. Francisco-Ortega, and R. K. Jansen, 1996 Hybridization and the extinction of rare plant species. Conservation biology **10**: 10–16.

Li, D., C. Li, Y. Yao, M. Li, and L. Liu, 2020 Modern imaging techniques in plant nutrition analysis: A review. Computers and Electronics in Agriculture **174**: 105459.

Li, M., M. H. Frank, and Z. Migicovsky, 2022 Colourquant: A high-throughput technique to extract and quantify color phenotypes from plant images. In *High-Throughput Plant Phenotyping: Methods and Protocols*, pp. 77–85, Springer.

Li, Z. and Y. Xu, 2022 Bulk segregation analysis in the ngs era: A review of its teenage years. The Plant Journal **109**: 1355–1374.

Lorensen, W. E. and H. E. Cline, 1987 Marching cubes: A high resolution 3d surface construction algorithm. ACM siggraph computer graphics **21**: 163–169.

Lowry, D. B., C. C. Sheng, J. R. Lasky, and J. H. Willis, 2012 Five anthocyanin polymorphisms are associated with an r2r3-myb cluster in mimulus guttatus (phrymaceae). American journal of botany **99**: 82–91.

Lowry, D. B., J. M. Sobel, A. L. Angert, T.-L. Ashman, R. L. Baker, *et al.*, 2019 The case for the continued use of the genus name mimulus for all monkeyflowers. Taxon **68**: 617–623.

Mähönen, A. P., K. t. Tusscher, R. Siligato, O. Smetana, S. Díaz-Triviño, *et al.*, 2014 Plethora gradient formation mechanism separates auxin responses. Nature **515**: 125–129.

Mallet, J., 2007 Hybrid speciation. Nature **446**: 279–283.

Marques, D. A., J. I. Meier, and O. Seehausen, 2019 A combinatorial view on speciation and adaptive radiation. Trends in ecology & evolution .

Martins, T. R., J. J. Berg, S. Blinka, M. D. Rausher, and D. A. Baum, 2013 Precise spatio-temporal regulation of the anthocyanin biosynthetic pathway leads to petal spot formation in clarkia gracilis (onagraceae). New Phytologist **197**: 958–969.

Martins, T. R., P. Jiang, and M. D. Rausher, 2017 How petals change their spots: cis-regulatory re-wiring in clarkia (onagraceae). New Phytologist **216**: 510–518.

MATLAB, 2017 *version 2017b*. The MathWorks Inc., Natick, Massachusetts.

McClintock, B., 1950 The origin and behavior of mutable loci in maize. Proceedings of the National Academy of Sciences **36**: 344–355.

Medel, R., A. Valiente, C. Botto-Mahan, G. Carvallo, F. Pérez, *et al.*, 2007 The influence of insects and hummingbirds on the geographical variation of the flower phenotype in mimulus luteus. Ecography **30**: 812–818.

Minervini, M., H. Scharr, and S. A. Tsaftaris, 2015 Image analysis: the new bottleneck in plant phenotyping [applications corner]. IEEE signal processing magazine **32**: 126–131.

Mukherjee, B. B. and R. K. Vickery, 1960 Chromosome counts in the section simiolus of the genus mimulus (scrophulariaceae). iv. Madroño **15**: 239–245.

Mukherjee, B. B. and R. K. Vickery, 1962 Chromosome counts in the section simiolus of the genus mimulus (scrophulariaceae). v. the chromosomal homologies of m. guttatus and its allied species and varieties. Madroño **16**: 141–155.

Nakano, A., H. Ikeno, T. Kimura, H. Sakamoto, M. Dannoura, *et al.*, 2012 Automated analysis of fine-root dynamics using a series of digital images. Journal of Plant Nutrition and Soil Science **175**: 775–783.

Neher, R. A. and O. Hallatschek, 2013 Genealogies of rapidly adapting populations. Proceedings of the National Academy of Sciences **110**: 437–442.

Petroni, K. and C. Tonelli, 2011 Recent advances on the regulation of anthocyanin synthesis in reproductive organs. Plant science **181**: 219–229.

Rieseberg, L. H., 1997 Hybrid origins of plant species. Annual review of Ecology and Systematics **28**: 359–389.

Rieseberg, L. H., O. Raymond, D. M. Rosenthal, Z. Lai, K. Livingstone, *et al.*, 2003 Major ecological transitions in wild sunflowers facilitated by hybridization. Science **301**: 1211–1216.

Sapir, Y., M. K. Gallagher, and E. Senden, 2021 What maintains flower colour variation within populations? Trends in Ecology & Evolution .

Schemske, D. W. and H. Bradshaw, 1999 Pollinator preference and the evolution of floral traits in monkeyflowers (mimulus). Proceedings of the National Academy of Sciences **96**: 11910–11915.

Schiedt, K., 1995 Isolation and analysis. Carotenoids **1**: 81–108.

Schwinn, K., J. Venail, Y. Shang, S. Mackay, V. Alm, *et al.*, 2006 A small family of myb-regulatory genes controls floral pigmen-

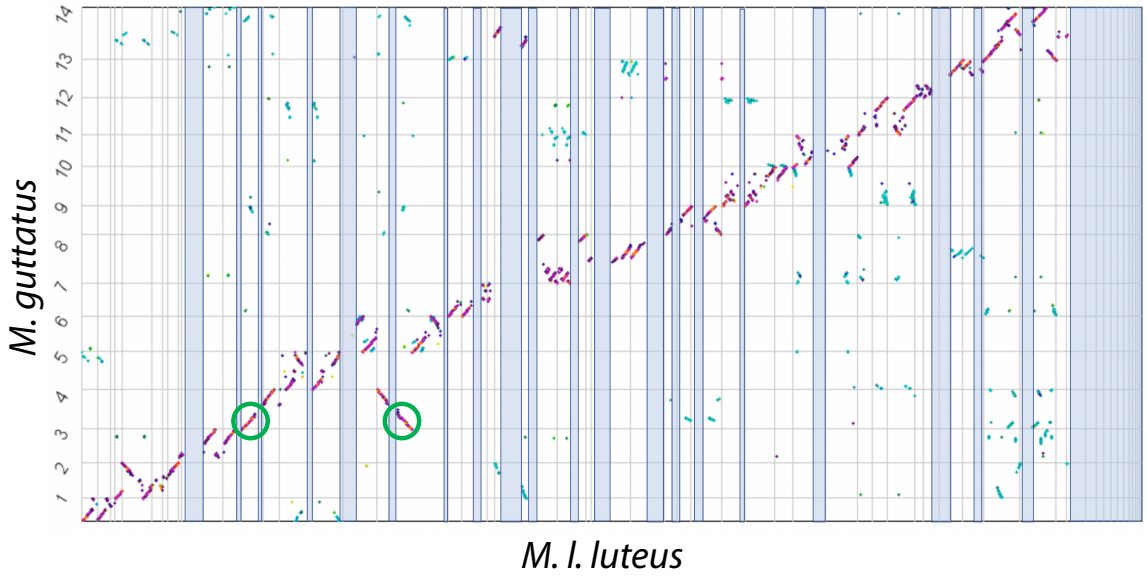

Figure 3 Syteny mapping between newly assembled *M. l. luteus* and publicly available *M. guttatus* genome reveals a whole-genome duplication in *M. l. luteus* and many missing portions in the *M. guttatus* assembly. The *M. l. luteus* genome is on the x-axis and *M. guttatus*, with numbers indicating chromosomes 1-14, is on the y-axis. Blue vertical boxes indicate portions of the *M. luteus* assembly that are missing in *M. guttatus*. The *M. l. luteus* whole genome duplication is clearly evident in this plot as each *M. guttatus* genomic portion is typically represented by two *M. l. luteus* genomic segments. For example, a large region on chromosome 4 in *M. guttatus* is present in two copies, inverted relative to each other, in *M. l. luteus* (green circles).

tation intensity and patterning in the genus antirrhinum. The Plant Cell **18**: 831–851.

Seehausen, O., 2004 Hybridization and adaptive radiation. Trends in ecology & evolution **19**: 198–207.

Smith, S. D., S. Wang, and M. D. Rausher, 2013 Functional evolution of an anthocyanin pathway enzyme during a flower color transition. Molecular biology and evolution **30**: 602–612.

Sobel, J. M. and M. A. Streisfeld, 2013 Flower color as a model system for studies of plant evo-devo. Frontiers in plant science **4**: 321.

Stanley, L. and Y.-W. Yuan, 2019 Transcriptional regulation of carotenoid biosynthesis in plants: so many regulators, so little consensus. Frontiers in Plant science **10**: 1017.

Stanton, K., C. M. Valentin, M. E. Wijnen, S. Stutstman, J. J. Palacios, *et al.*, 2016 Absence of postmating barriers between a selfing vs. outcrossing chilean mimulus species pair. American journal of botany **103**: 1030–1040.

Stracke, R., M. Werber, and B. Weisshaar, 2001 The r2r3-myb gene family in arabidopsis thaliana. Current opinion in plant biology **4**: 447–456.

Streisfeld, M. A., W. N. Young, and J. M. Sobel, 2013 Divergent selection drives genetic differentiation in an r2r3-myb transcription factor that contributes to incipient speciation in mimulus aurantiacus. PLoS genetics **9**: e1003385.

Suarez-Gonzalez, A., C. Lexer, and Q. C. Cronk, 2018 Adaptive introgression: a plant perspective. Biology letters **14**: 20170688.

Takahashi, Y., K.-i. Takakura, and M. Kawata, 2015 Flower color polymorphism maintained by overdominant selection in sisyrinchium sp. Journal of plant research **128**: 933–939.

Tanaka, H., P. Dhonukshe, P. Brewer, and J. Friml, 2006 Spatiotemporal asymmetric auxin distribution: a means to coordinate plant development. Cellular and Molecular Life Sciences CMLS **63**: 2738–2754.

Trivellini, A., B. Gordillo, F. J. Rodriguez-Pulido, E. Borghesi, A. Ferrante, *et al.*, 2014 Effect of salt stress in the regulation of anthocyanins and color of hibiscus flowers by digital image analysis. Journal of agricultural and food chemistry **62**: 6966–6974.

Twyford, A. D., A. M. Caola, P. Choudhary, R. Raina, and J. Friedman, 2018 Loss of color pigmentation is maintained at high frequency in a monkey flower population. The American Naturalist **191**: 135–145.

Van der Walt, S., J. L. Schönberger, J. Nunez-Iglesias, F. Boulogne, J. D. Warner, *et al.*, 2014 scikit-image: image processing in python. PeerJ **2**: e453.

Vickery, R., K. Crook, D. Lindsay, M. Mia, and W. Tai, 1968 Chromosome counts in section simiolus of the genus mimulus (scrophulariaceae). vii. new numbers for m. guttatus, m. cupreus, and m. tilingii. Madroño **19**: 211–218.

Vickery, R. K., 1995 Speciation by aneuploidy and polyploidy in mimulus (scrophulariaceae). The Great Basin Naturalist **55**: 174–176.

Virtanen, P., R. Gommers, T. E. Oliphant, M. Haberland, T. Reddy, *et al.*, 2020 SciPy 1.0: Fundamental Algorithms for Scientific Computing in Python. Nature Methods **17**: 261–272.

Von Bohlen, C., 1995 El género mimulus l.(scrophulariaceae) en chile. Gayana Botanica **52**: 7–28.

Watson, J. M. and C. Von Bohlen, 2000 Plate 400. mimulus naiandinus. Curtis's Botanical Magazine **17**: 195–201.

Weight, C., D. Parnham, and R. Waites, 2008 Technical advance: Leafanalyser: a computational method for rapid and large-scale analyses of leaf shape variation. The Plant Journal **53**: 578–586.

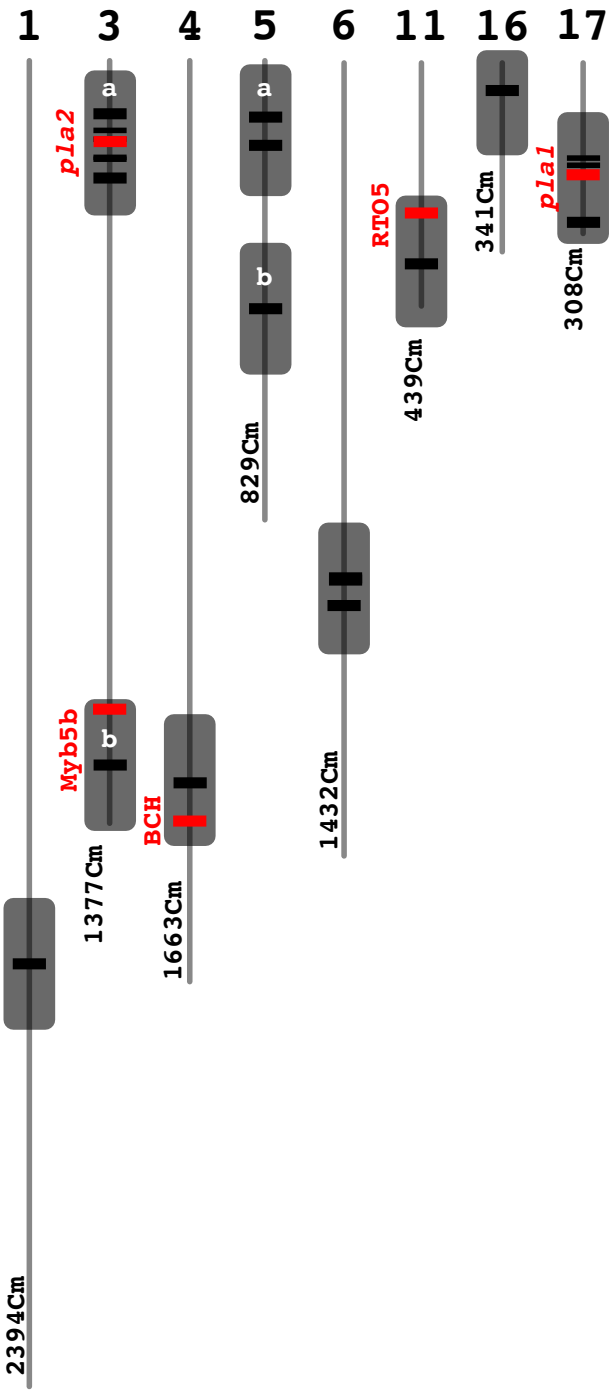

Figure 4 QTL mapping revealed ten statistically significant peaks, nine of which were associated with anthocyanin pigmentation and one of which was associated with carotenoid pigmentation. Linkage group numbers, also used to name the QTLs, are shown at the top of each linkage group. The length of the linkage group in centiMorgans is shown at the bottom. The *pla1* genomic region at QTL-3a harbors anthocyanin-activating transcription factor *MYB5a/NEGAN*, shown to be the single gene required to activate petal lobe anthocyanin pigmentation in *M. l. variegatus* (Zheng *et al.* 2021). A putative duplicate copy of *MYB5a* is found at QTL-3b. The *pla2* genomic region at QTL-17 contains seven tandemly arrayed putatively anthocyanin-related *MYB1-3* gene copies (Cooley *et al.* 2011). QTL-11 contains candidate gene *RTO5*, which BLASTs to the *RED TONGUE* gene that is a repressor of *MYB5a/NEGAN* (Ding *et al.* 2020). QTL-4 contains the carotenoid biosynthetic enzyme *Beta-carotene hydroxylase (BCH)*.

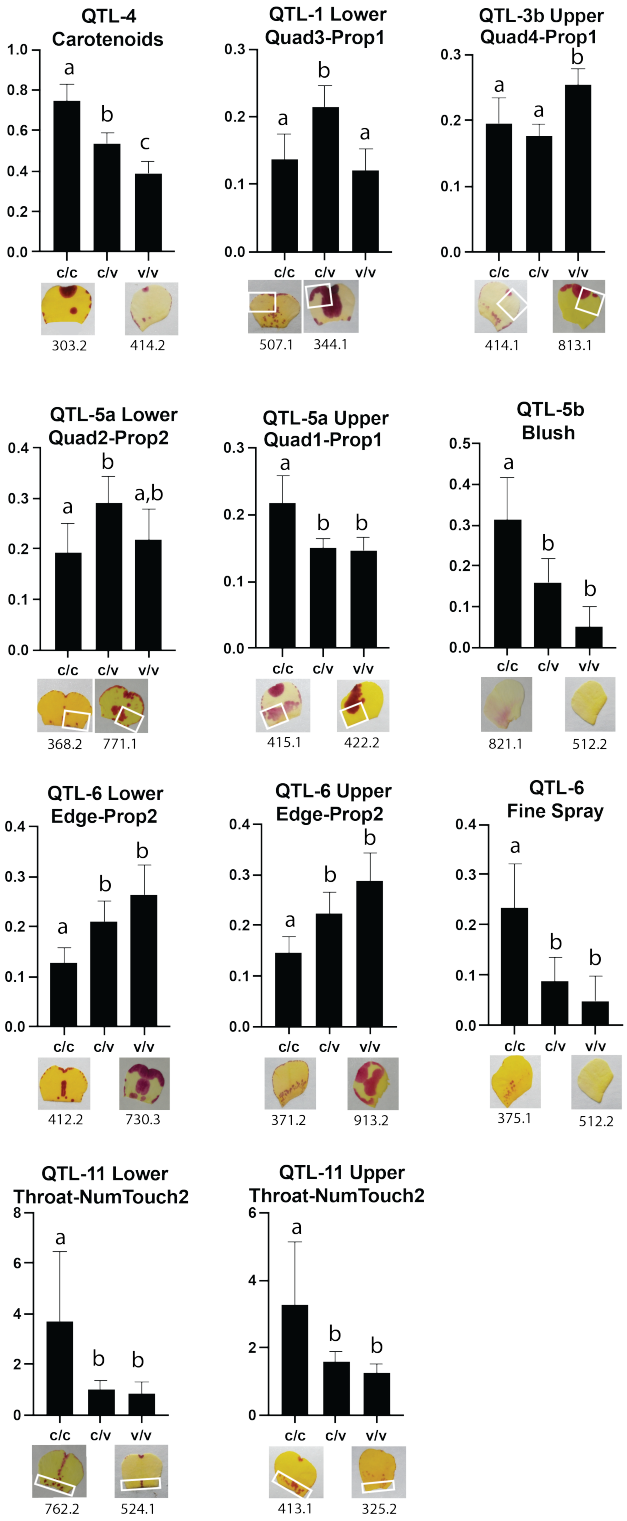

Figure 5 Most anthocyanin and carotenoid patterning QTLs were associated with 1-3 patterning traits each. For each graph, the QTL (named for the linkage group to which it maps) is given, followed by "Lower" or "Upper" for traits that were measured separately for lower and upper petals. Abbreviated trait names are stated in the second line, and are described in Table 3. c/c, c/v, and v/v indicate genotype (c, *cupreus* allele; v, *variegatus* allele), with representative images shown below. White rectangles show approximate locations of quadrants and throat region. Error bars are 95% confidence intervals.

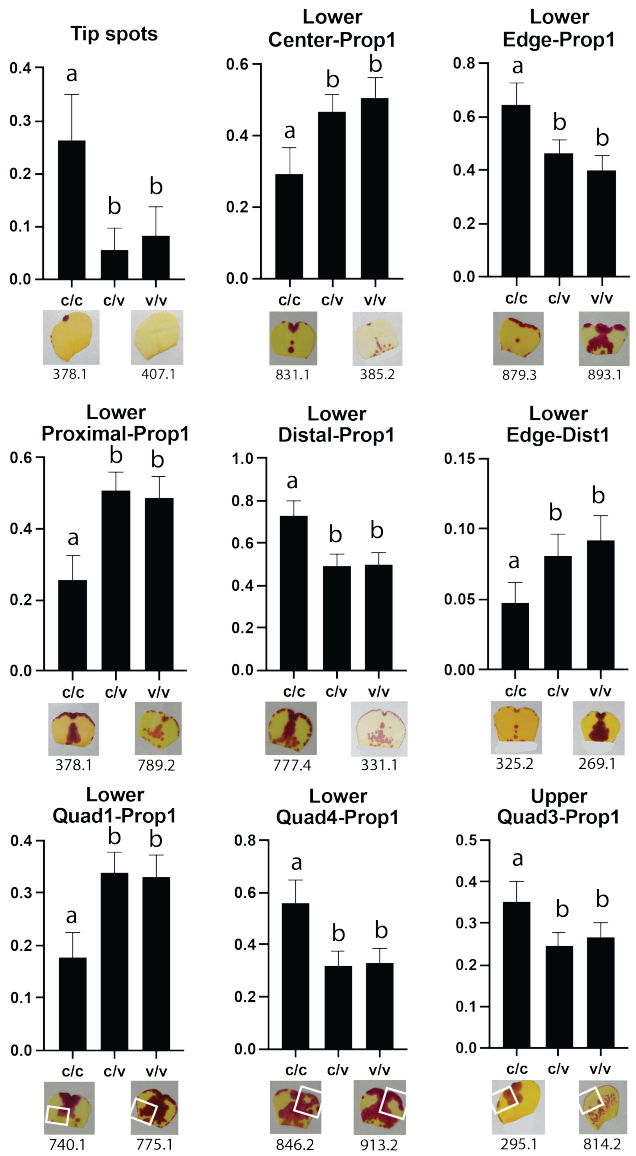

Figure 6 An anthocyanin patterning QTL on linkage group 17 was associated with nine patterning traits. "Lower" and "Upper" refer to lower (ventral) versus upper (dorsal) petals. Abbreviated trait names are shown above each graph, and are described in Table 3. c/c, c/v, and v/v indicate genotype (c, *cupreus* allele; v, *variegatus* allele), with representative images shown below. hite rectangles show approximate locations of quadrants. Error bars are 95% confidence intervals.

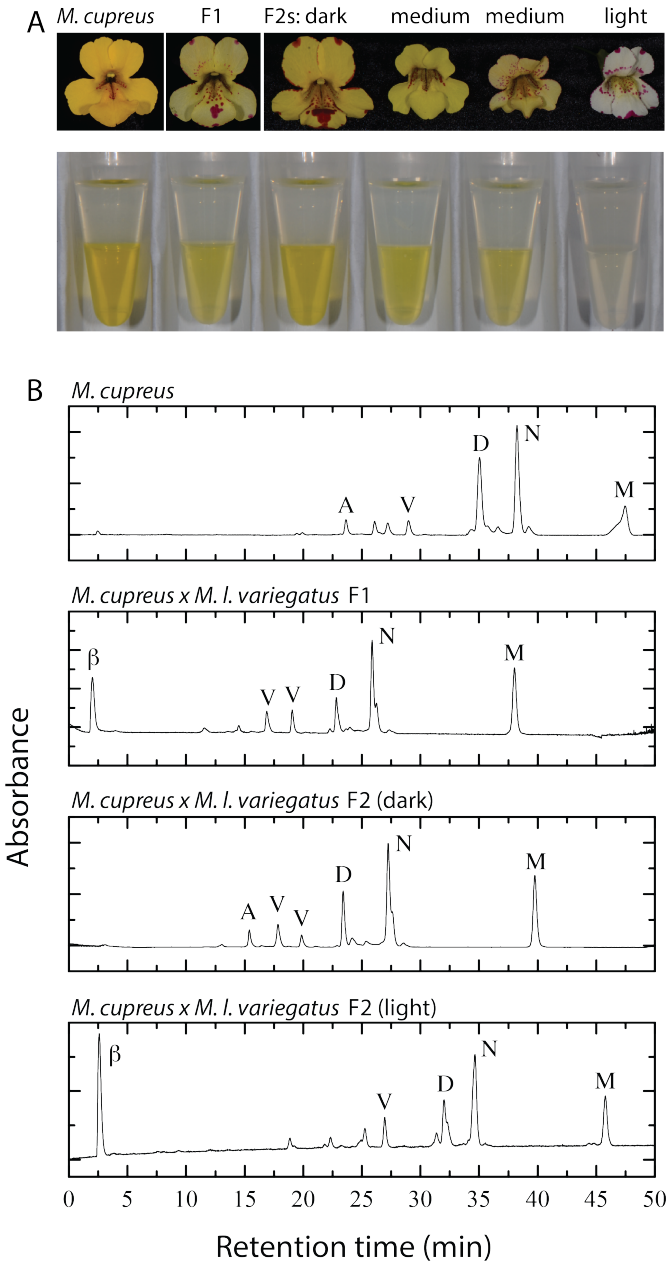

Figure 7 Intensity of yellow pigmentation corresponds with shifts in carotenoid composition. A. The *M. cupreus* parent, *M. cupreus* x *M. l. variegatus* F1 hybrid, a dark F2 individual (third from left), and a pale-yellow individual (fifth from left) were used for liquid phase partitioning of flavonoids and carotenoids as shown in the bottom panel. B. HPLC chromatograms of floral extracts. Abbreviations are as follows: A, antheraxanthin; B, beta-carotene; D, deepoxyneoxanthin; M, mimulaxanthin; N, neoxanthin; V, violaxanthin.

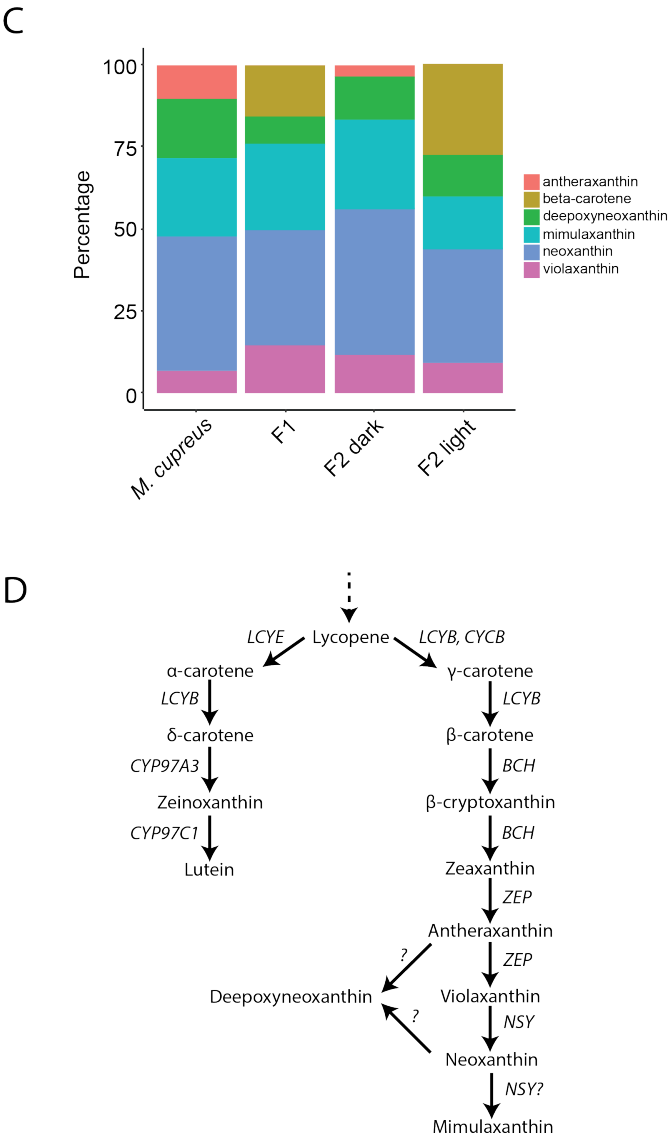

Figure 8 (Figure 7, continued). C. Relative percentages of carotenoids as determined by integration of HPLC peak areas. D. A partial carotenoid pathway based on LaFountain *et al.* (2015) and Stanley and Yuan (2019).

Wu, C., D. Lowry, A. Cooley, K. Wright, Y. Lee, *et al.*, 2008 Mimulus is an emerging model system for the integration of ecological and genomic studies. Heredity **100**: 220.

Xu, W., C. Dubos, and L. Lepiniec, 2015 Transcriptional control of flavonoid biosynthesis by myb–bhlh–wdr complexes. Trends in plant science **20**: 176–185.

Yamagishi, M., 2013 How genes paint lily flowers: regulation of colouration and pigmentation patterning. Scientia Horticulturae **163**: 27–36.

Yamagishi, M., S. Toda, and K. Tasaki, 2014 The novel allele of the lh myb 12 gene is involved in splatter-type spot formation on the flower tepals of asiatic hybrid lilies (lilium spp.). New Phytologist **201**: 1009–1020.

Yamamizo, C., S. Kishimoto, and A. Ohmiya, 2010 Carotenoid composition and carotenogenic gene expression during ipomoea petal development. Journal of experimental botany **61**: 709–719.

Yoshioka, Y., H. Iwata, R. Ohsawa, and S. Ninomiya, 2004 Quantitative evaluation of flower colour pattern by image analysis and principal component analysis of primula sieboldii e. morren. Euphytica **139**: 179–186.

Yuan, Y.-W., 2019 Monkeyflowers (mimulus): new model for plant developmental genetics and evo-devo. New Phytologist **222**: 694–700.

Yuan, Y.-W., J. M. Sagawa, L. Frost, J. P. Vela, and H. D. Bradshaw Jr, 2014 Transcriptional control of floral anthocyanin pigmentation in monkeyflowers (*Mimulus*). New Phytologist **204**: 1013–1027.

Zhao, C., X.-Q. Wang, and F.-S. Yang, 2014 Mechanisms underlying flower color variation in asian species of meconopsis: A preliminary phylogenetic analysis based on chloroplast dna and anthocyanin biosynthesis genes. Journal of Systematics and Evolution **52**: 125–133.

Zheng, X., K. Om, K. A. Stanton, D. Thomas, P. A. Cheng, *et al.*, 2021 The regulatory network for petal anthocyanin pigmentation is shaped by the myb5a/negan transcription factor in mimulus. Genetics **217**: iyaa036.

Zhou, X., R. McQuinn, Z. Fei, A.-M. A. WOLTERS, J. Van Eck, *et al.*, 2011 Regulatory control of high levels of carotenoid accumulation in potato tubers. Plant, Cell & Environment **34**: 1020–1030.